Front. Earth Sci. 2019, 13(1): 124–131
https://doi.org/10.1007/s11707-018-0698-8

RESEARCH ARTICLE

Estimation of wind speeds inside Super Typhoon Nepartak from AMSR2 low-frequency brightness temperatures

Lei ZHANG[1], Xiaobin YIN (✉)[2], Hanqing SHI[1], Zhenzhan WANG[3], Qing XU[4]

1 Institute of Meteorology and Oceanography, National University of Defense Technology, Nanjing 211101, China
2 Beijing Piesat Information Technology Co. Ltd, Beijing 100195, China
3 National Space Science Center, Chinese Academy of Sciences, Beijing 100190, China
4 College of Oceanography, Hohai University, Nanjing 211101, China

Abstract Accurate estimations of typhoon-level winds are highly desired over the western Pacific Ocean. A wind speed retrieval algorithm is used to retrieve the wind speeds within Super Typhoon Nepartak (2016) using 6.9- and 10.7-GHz brightness temperatures from the Japanese Advanced Microwave Scanning Radiometer 2 (AMSR2) sensor on board the Global Change Observation Mission-Water 1 (GCOM-W1) satellite. The results show that the retrieved wind speeds clearly represent the intensification process of Super Typhoon Nepartak. A good agreement is found between the retrieved wind speeds and the Soil Moisture Active Passive wind speed product. The mean bias is 0.51 m/s, and the root-mean-square difference is 1.93 m/s between them. The retrieved maximum wind speeds are 59.6 m/s at 04:45 UTC on July 6 and 71.3 m/s at 16:58 UTC on July 6. The two results demonstrate good agreement with the results reported by the China Meteorological Administration and the Joint Typhoon Warning Center. In addition, Feng-Yun 2G (FY-2G) satellite infrared images, Feng-Yun 3C (FY-3C) microwave atmospheric sounder data, and AMSR2 brightness temperature images are also used to describe the development and structure of Super Typhoon Nepartak.

Keywords microwave radiometer, sea surface wind retrieval, AMSR2, Nepartak, SMAP

1 Introduction

The northwestern Pacific Ocean is one of the most active ocean basins, as tropical cyclones strike the most frequently therein. A typhoon, as a type of severe tropical cyclone, can produce fierce winds and heavy rains as well as high waves and damaging storm surges that can produce dramatic impacts on the safety of both life and property. Using a combination of forecast models, satellite imagery, and data analysis, tropical cyclone tracking and forecasting have achieved remarkable advancements over the last decades (Roy and Kovordányi, 2012). However, the accuracies of tropical cyclone intensity forecasts have seen much less progress over the same period.

Passive microwave radiometers have been used to retrieve ocean parameters (e.g., the wind speed, sea surface temperature, and sea surface salinity) for a long time (Goodberlet et al., 1990; Krasnopolsky et al., 1995; Wentz, 1997; Yueh et al., 2006; Zhang et al., 2016a). Previous research has demonstrated that microwave radiometers can be used to retrieve wind speeds with an accuracy of approximately 1 m/s when the weather conditions are clear. Retrieval algorithms can be divided into two categories: statistical algorithms and physical-based algorithms. Statistical algorithms always employ regression or neural networks (NN) techniques to retrieve wind speeds with matching brightness temperatures (Goodberlet et al., 1990; Krasnopolsky et al., 1995; Wentz and Meissner, 2000). Physical-based algorithms use a radiative transfer model that relates brightness temperatures to retrieved geophysical parameters, such as the wind speed and sea surface temperature (Wentz, 1997). However, the performances of these algorithms break down completely when rain is present (Meissner and Wentz, 2009). Rain increases the atmospheric attenuation, especially at higher frequencies (e.g., 37 GHz). In fact, the brightness temperatures at higher frequencies are nearly saturated near the eyes of hurricanes (Yueh, 2008). In addition, it is very difficult to accurately model brightness temperatures under rainy conditions because of the high variability within rainy

Received September 29, 2017; accepted December 18, 2017

E-mail: yinxiaobin@piesat.cn

atmospheres and the complicated dielectric properties of the ocean surface (Meissner and Wentz, 2009; Zabolotskikh et al., 2015).

One of the most important applications of radiometers is the study of severe ocean weather systems (Quilfen et al., 2007). Previous investigations noted that brightness temperatures from low-frequency channels (such as the L-band and C-band) can be used to retrieve wind speeds under extreme conditions such as tropical cyclones (Shibata, 2006; Uhlhorn et al., 2007; Yan and Weng, 2008; Meissner and Wentz, 2009; Reul et al., 2012). The Stepped Frequency Microwave Radiometer (SFMR), which is a typical airborne sensor onboard National Oceanic Atmospheric Administration (NOAA) aircraft, has been successfully used to estimate wind speed in hurricanes (Uhlhorn and Black, 2003). However, reconnaissance aircraft missions are mainly focused on the North Atlantic Ocean and the eastern Pacific Ocean. Little has been reported about the retrieval of tropical cyclone intensities over the northwestern Pacific Ocean.

The AMSR2 instrument is a conically scanning passive microwave radiometer on board the JAXA GCOM-W1 spacecraft, which was launched on May 18, 2012. AMSR2 provides TB observations at frequencies ranging from 6.9 to 89 GHz and is equipped entirely with dual-polarization channels. AMSR2 low-frequency brightness temperatures have been used to study wind speed retrievals in extratropical cyclones (Zabolotskikh et al., 2014). Super Typhoon Nepartak (2016), a Category-5 hurricane, struck the northwestern Pacific Ocean and had disastrous effects in Taiwan and Fujian. The AMSR2 sensor successfully captured four images when the development of Super Typhoon Nepartak was vigorous during July 5–7. In this paper, a new algorithm was established and used to retrieve wind speeds inside Super Typhoon Nepartak over the northwestern Pacific Ocean.

This paper is organized as follows. Section 2 describes the development and structure of Super Typhoon Nepartak. The retrieval algorithm is presented in Section 3. Section 4 tests the performance of the retrieval algorithm for Super Typhoon Nepartak and compares the retrieval results with the Soil Moisture Active Passive (SMAP) wind speed product. The conclusions are presented in Section 5.

2 Description of Super Typhoon Nepartak

The genesis of Super Typhoon Nepartak can be traced back to a low-pressure area that emerged from the south of Guam on June 30, 2016. After a period of slow development, it was estimated that a tropical depression formed on July 2. Shortly afterwards, the Joint Typhoon Warning Center (JTWC) issued a tropical cyclone formation alert. By 3 July, the Japan Meteorological Agency (JMA) upgraded the system to a tropical storm and named it Nepartak. The path of Nepartak is shown in Fig. 1, and the time series of the maximum wind speed and the minimum central pressure are also displayed in Fig. 1.

Nepartak followed along a west-northwestward heading during its lifetime. On July 3, its forward speed was approximately 15–20 km/h. By July 4, it had started to accelerate up to 30 km/h under the influence of a subtropical ridge. At approximately 12:00 UTC on July 4, the JMA upgraded it to a severe tropical storm. Both the CMA and the JMA upgraded Nepartak to a typhoon on July 5; its annular characteristics can be found in Feng-Yun-2G (FY-2G) satellite infrared images displayed in Fig. 2(a). On the evening of July 5, due to a low vertical

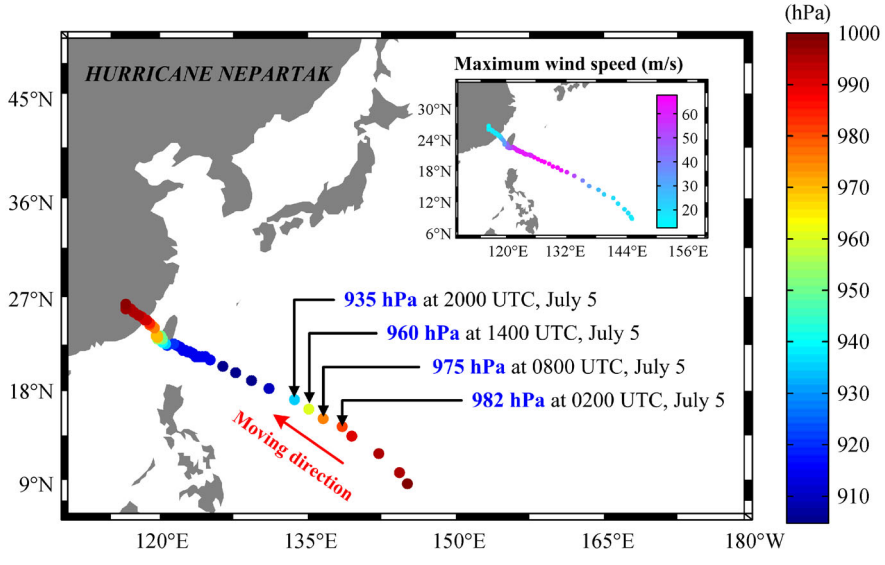

Fig. 1 The best track positions, minimum central pressure, and maximum wind speed for Super Typhoon Nepartak during July 3–10, 2016, based on analyses from the China Meteorological Administration (CMA) typhoon website.

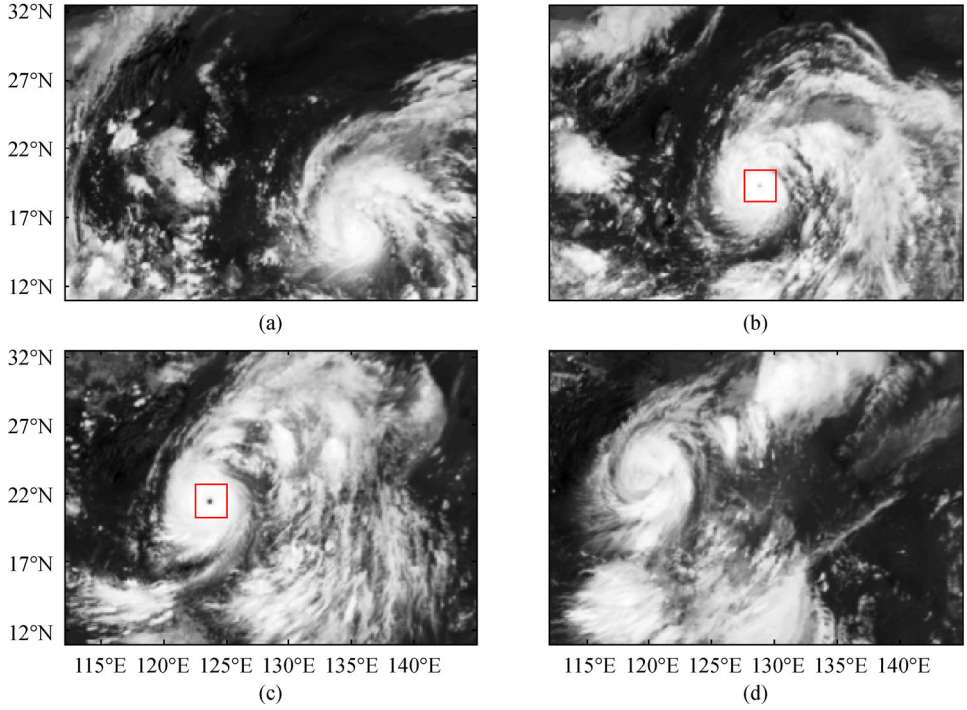

Fig. 2 FY-2G satellite infrared images over Super Typhoon Nepartak (a) at 05:00 UTC on July 5, 2016; (b) at 05:00 UTC on July 6, 2016; (c) at 05:00 UTC on July 7, 2016; and (d) at 05:00 UTC on July 8, 2016.

wind shear and warm sea surface temperature (above 30°C), a needle-like eye was formed which is obvious in Figs. 2(b) and 2(c). The JTWC upgraded it to a Category 4-equivalent super typhoon on July 5. The central pressure decreased by approximately 47 hPa/24 h on July 5. On July 6, Nepartak reached its peak intensity and was classified as a Category 5-equivalent super typhoon. Nepartak made landfall over Taiwan on July 8. The compact and symmetric annular characteristics acquired by the typhoon are obvious in Fig. 2(d).

The evolution of the structure of Nepartak can also be found in Figs. 3(a)–3(c). These figures show the observed AMSR2 6.9- and 10.7-GHz brightness temperature measurements over two continuous days (July 5–6). With an increase in the intensity, the observed brightness temperatures gradually increased near the typhoon eye. The annular and symmetric characteristics are also obvious in Fig. 3(c).

The Advanced Microwave Atmospheric Sounder (AMAS) on board the FY-3C represents the new generation of the Microwave Humidity Sounder (MWHS) instrument and follows the heritage and development of the MWHS sensor on board the FY-3(A/B) satellite (He et al., 2015). AMAS was designed for global atmospheric humidity and temperature measurements under all-weather conditions. It plays an important role in monitoring extreme climate conditions. The images of Nepartak were captured by FY-3C, and the vertical structure of Super Typhoon Nepartak can be found in Fig. 4.

3 Method

Some statistical algorithms have been used to retrieve hurricane wind speeds (Shibata, 2006; Meissner and Wentz, 2009; Zabolotskikh, et al., 2014; Zhang et al., 2016b). Since the brightness temperature signals of rain and wind are very similar, these algorithms always use a channel combination of brightness temperatures in order to make the brightness temperature signals sensitive to the wind speed and less sensitive to rain. A previous study proposed an improved algorithm to retrieve high wind speeds inside hurricanes, and the algorithm was applied with encouraging accuracy to WindSat brightness temperature measurements for wind speed retrievals (Zhang et al., 2016b). Two new brightness temperature increments ($W6H$ and $W6V$) for wind speed estimates inside hurricanes were defined as follows:

$$W6H = (6H^- - c_1 \times 10H^- + a_1 \times c_1 - b_1) \times \frac{\frac{sl_1}{(sl_1 - c_1)}}{fac_1}, \quad (1)$$

$$sl_1 = d_1 + e_1 \times (10H_E^- - a_1), \quad (2)$$

$$fac_1 = 1 - f_1 \times (10H_E^- - a_1), \quad (3)$$

$$6(10)H^- = \text{Satellite}_{6(10)H} - \text{CalmOcean}_{6(10)H}, \quad (4)$$

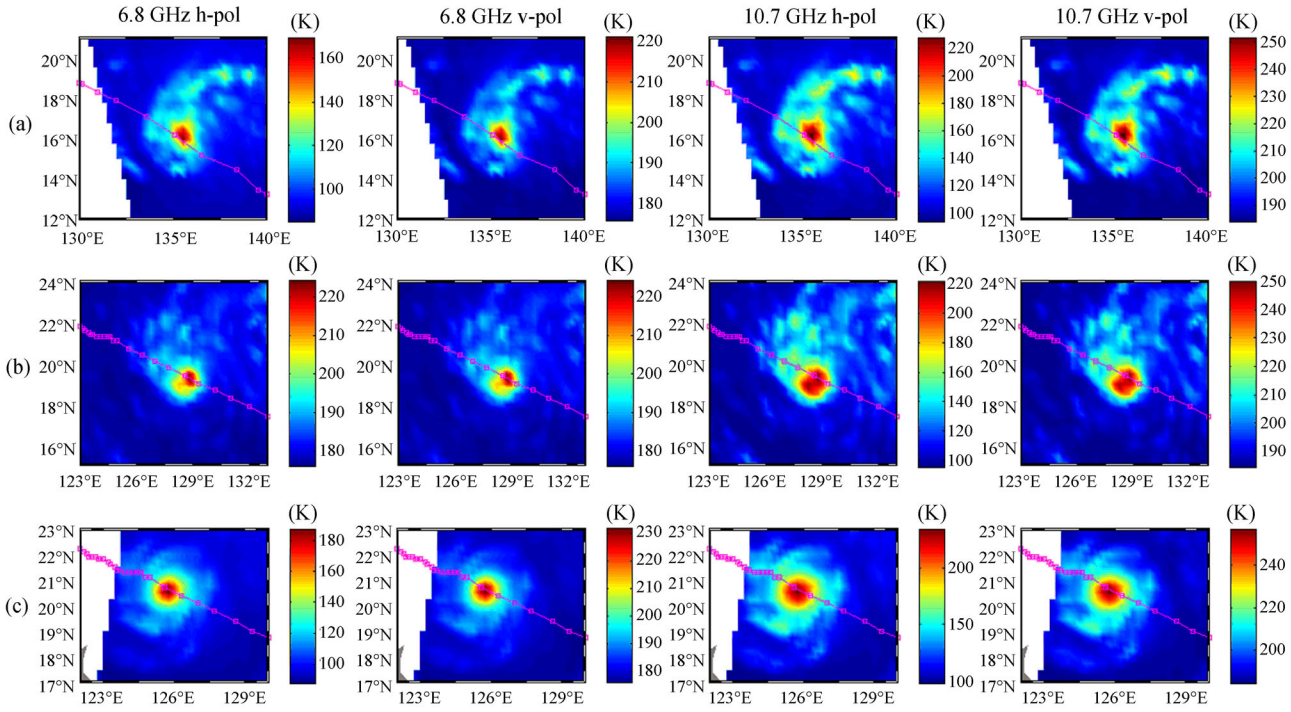

Fig. 3 The GCOM-W1 AMSR2 observed 6.9- and 10.7-GHz brightness temperature measurements over Super Typhoon Nepartak at (a) approximately 04:03 UTC on July 5, 2016; (b) approximately 04:46 UTC on July 6, 2016; and (c) approximately 16:58 UTC on July 6, 2016. The hollow pink squares represent the best track positions of Super Typhoon Nepartak based on analyses from the CMA typhoon website.

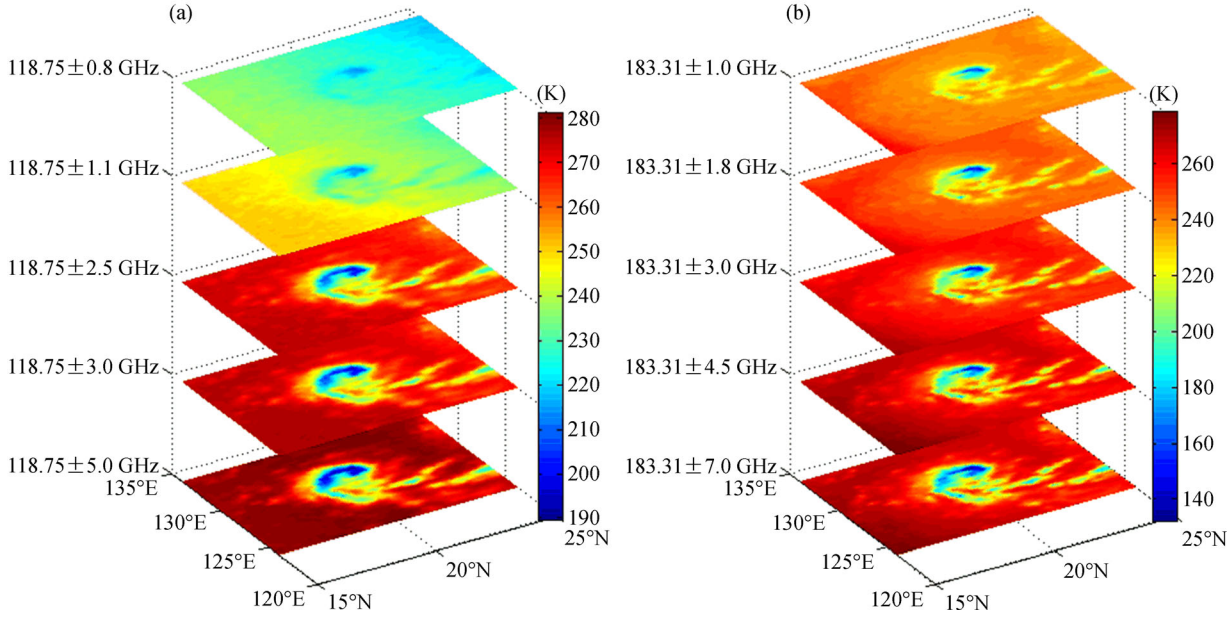

Fig. 4 The FY-3C observed brightness temperatures over Super Typhoon Nepartak on July 6, 2016.

$$W6V = (6V^{-} - c_2 \times 10V^{-} + a_2 \times c_2 - b_2) \times \frac{\frac{sl_2}{(sl_2 - c_2)}}{fac_2}, \quad (5)$$

$$sl_2 = d_2 + e_2 \times (10V_E^{-} - a_2), \quad (6)$$

$$fac_2 = 1 - f_2 \times (10V_E^{-} - a_2), \quad (7)$$

$$6(10)V^{-} = \text{Satellite}_{6(10)V} - \text{CalmOcean}_{6(10)V}, \quad (8)$$

where $a_i \sim f_i$ ($i = 1,2$) are the undetermined coefficients, and the meaning of the parameters can be found in the literature (Zhang et al., 2016b). Satellite_6(10)P is the brightness temperature measurement for the 6(10)-GHz channel with a polarization of P (P = V, H), and CalmOcean_6(10)P is the ocean emission for 6(10)-GHz channel under calm ocean conditions. The parameters $10H_E^{-}$ and $10V_E^{-}$ can be calculated using an iterative method (Zhang et al., 2016b). Finally, a new algorithm was developed that relates *W6H* and *W6V* to the wind speeds (m/s) inside hurricanes.

$$\begin{aligned} WS &= m_1 \times W6H + m_2 \times W6V + m_3 && \text{if } W6H < n_1 \\ WS &= m_4 \times (W6H - n_1) + m_5 \times (W6V - n_2) + m_6 && \text{if } n_1 \leqslant W6H < n_2 \\ WS &= m_7 \times (W6H - n_2) + m_8 \times (W6V - n_2 - 10) + m_9 && \text{if } W6H \geqslant n_2 \end{aligned} \quad (9)$$

Some differences (e.g., in the frequency, Earth incidence angle, and calibration method) can be found among different space-borne microwave radiometers. Therefore, we need to retrain this model for a special sensor. In the research reported in this paper, we used the two brightness temperature increments *W6H* and *W6V* to retrieve the wind speeds inside hurricanes using AMSR2 measurements. To obtain the coefficients in Eqs. (1)–(9), we collected AMSR2 brightness temperature observations of 23 tropical cyclones and SFMR measurements during the period from 2012 to 2015. Subsequently, we created a simple moving average of SFMR along-track wind speeds using every 20 sample points, which enabled us to obtain SFMR measurements with a spatial resolution of 30 km along the flight track. A 15-km spatial window and a 25-min temporal window were used to create the collocation between the AMSR2 measurements and SFMR wind speeds.

4 Results

4.1 Wind speed retrieval model for AMSR2

The wind speed retrieval model was finally established using 8551 matchups between the AMSR2 measurements and SFMR wind speeds, resulting in a mean bias and an RMS difference of −0.12 m/s and 3.25 m/s, respectively. The results are shown in Fig. 5. The model coefficients in Eqs. (1)–(9) can be found in Table 1.

4.2 Application to Super Typhoon Nepartak

Nepartak formed as a typhoon on July 5 with an estimated maximum wind speed of 52 m/s at 20:00 UTC based on the China Meteorological Administration (CMA) typhoon website. After Nepartak strengthened and reached its peak intensity with a needle-like eye on July 6, as can be observed in Fig. 2(b), the estimated maximum wind speed was approximately 68 m/s according to the CMA typhoon website. Three images about it were effectively captured by the GCOM-W1 AMSR2 sensor during July 5 – 6, 2016. Based on the method described in Section 3, we retrieved the wind speeds inside Super Typhoon Nepartak using the GCMO-W1 AMSR2 6.9- and 10.7-GHz brightness temperatures. Figures 6(a) – 6(c) illustrates the retrieved wind speeds using our new model. This sequence of figures clearly shows the intensification process of Super Typhoon Nepartak. The retrieved maximum wind speed was 49.8 m/s at 04:02 UTC on July 5. Nepartak strengthened on July 6, and the retrieved maximum wind speed was approximately 59.6 m/s at 04:45 UTC. This value is slightly lower than the value of approximately 60 m/s at 02:00 UTC reported by the CMA typhoon website. After Super Typhoon Nepartak further strengthened, the retrieved maximum wind speed was 71.3 m/s at 16:58 UTC on July 6. On July 6, Nepartak became a Category 5-equivalent super typhoon. These results show good agreement with the report published by the Joint Typhoon Warning Center (JTWC) on July 6.

The validation of hurricane surface wind fields is

Table 1 Model coefficients in Eqs. (1)–(9)

a_1	b_1	c_1	d_1	e_1	f_1	a_2	b_2	c_2	d_2	e_2	f_2
23.4021	0.3119	0.2438	0.9776	0.0144	0.0005	10.1119	0.0019	0.4067	1.0000	0.0100	0.0005
m_1	m_2	m_3	m_4	m_5	m_6	m_7	m_8	m_9	n_1	n_2	
0.1300	0.1000	18.0000	0.005	0.0528	9.3693	0.8975	0.0500	11.2458	20	30	

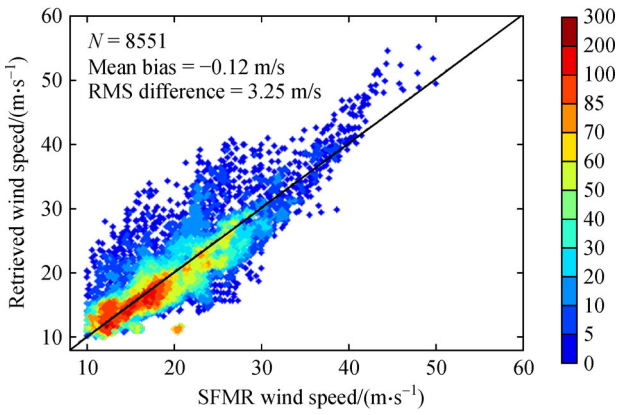

Fig. 5 SFMR wind speed retrieval results versus the retrieved wind speeds using the AMSR2 measurements. The color denotes the number of pixels that contributed to the scatter plots.

inherently challenging because there is no realizable "surface truth" data. In recent years, some reconnaissance aircraft missions have been carried out over the Atlantic Ocean and the eastern Pacific Ocean to observe hurricanes, and those missions can provide along-track wind speed measurements up to 70 m/s (Uhlhorn, et al., 2007). Unfortunately, such reconnaissance aircraft missions have not been flown over the western Pacific Ocean in recent years.

In this study, we selected SMAP sea surface wind speeds as a candidate to compare our retrieved results. SMAP wind speed products (Meissner et al., 2016) are produced by Remote Sensing Systems (RSS) using L-band brightness temperatures, and the development of the SMAP wind retrieval algorithm is still ongoing. Three very intense cyclones were used to illustrate its capability. A detailed description of the storm Winston (Fiji Islands, February 2016) can be found on the RSS website. It should be noted that there is an approximately 5-h interval between the AMSR2 and SMAP measurements. Within this 5-h time window, a hurricane could move over a relatively large distance. Therefore, we shifted the SMAP data to coincide with the eye of the AMSR2 measurements. Finally, the collocation contained 768 matchups between them. The results show a mean bias of 0.51 m/s and a root-mean-square difference of 1.93 m/s between them. The retrieved wind speeds show good agreement with the SMAP data. Figure 7(b) shows the SMAP wind speed results at approximately 09:13 UTC on July 5, 2016, and Figure 7(c) shows the SMAP wind speed results at approximately 21:58 UTC on July 6, 2016. The maximum wind speed was 70.15 m/s at 21:58 UTC, which indicates good agreement with our retrieved results.

5 Conclusions

In this paper, we tested an improved algorithm for the retrieval of super typhoon wind speeds over the western Pacific Ocean using AMSR2 low-frequency brightness temperature measurements. The results indicate that the retrieved wind speeds clearly represent the intensification process of Super Typhoon Nepartak. On July 6, Super Typhoon Nepartak reached its peak intensity and became a Category 5-equivalent super typhoon. The retrieved maximum wind speeds were 59.6 m/s at 04:45 UTC and 71.3 m/s at 16:58 UTC. These results show good agreement with the results reported by the CMA and JTWC. Furthermore, we also compared the retrieved results with the SMAP wind speed product which has been

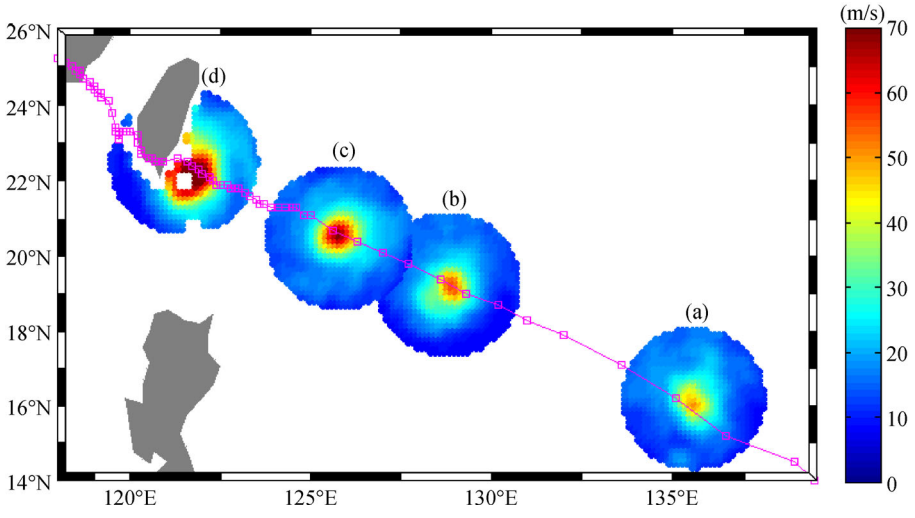

Fig. 6 Wind speed retrieval results from our new algorithm using the GCOM-W1 AMSR2 observed 6.9- and 10.7-GHz brightness temperatures over Super Typhoon Nepartak at (a) approximately 04:02 UTC on July 5, 2016; (b) approximately 04:46 UTC on July 6, 2016; (c) approximately 16:58 UTC on July 6, 2016; and (d) approximately 17:40 UTC on July 7, 2016. The hollow pink squares represent the best track positions for Super Typhoon Nepartak based on analyses from the CMA typhoon website.

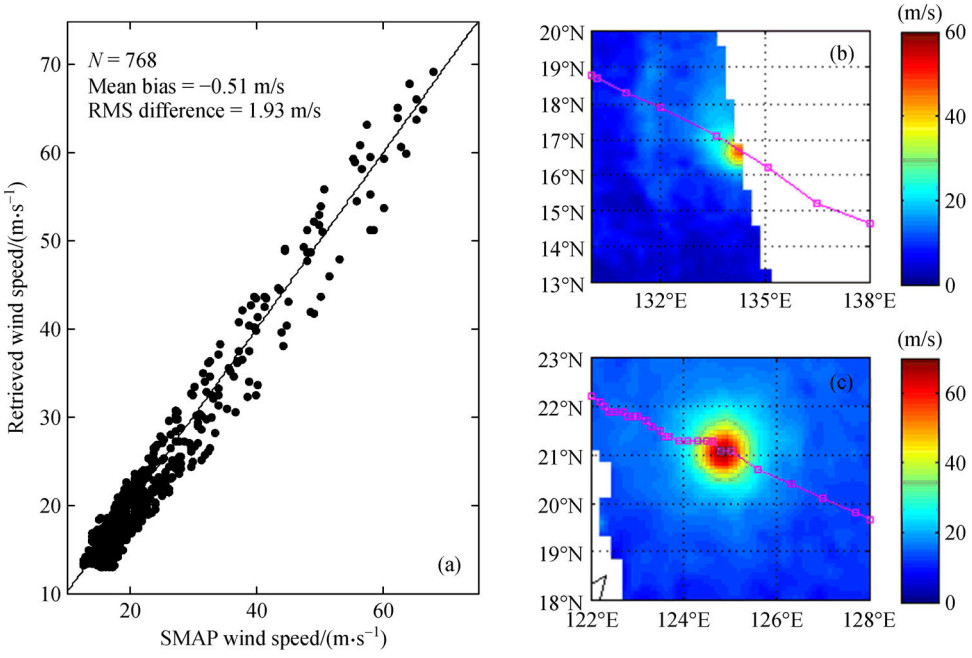

Fig. 7 (a) SMAP wind speed retrievals versus AMSR2 retrieval results. (b) SMAP wind speed retrievals from the RSS over Super Typhoon Nepartak at approximately 09:13 UTC on July 5, 2016. (c) SMAP wind speed retrievals from the RSS over Super Typhoon Nepartak at approximately 21:58 UTC on July 6, 2016. The hollow pink squares represent the best track positions for Super Typhoon Nepartak based on analyses from the CMA typhoon's website.

used to study higher wind speeds and has obtained some significant results. The mean bias was 0.51 m/s and the root-mean-square difference was 1.93 m/s between them. The maximum wind speed retrieved using SMAP product was 70.15 m/s at 21:58 UTC on July 6, which indicates a good agreement with our retrieved results. In addition, the retrieved maximum wind result (49.8 m/s) shows good agreement with the SMAP result (49.7 m/s) on July 5.

The improved algorithm can be used to retrieve hurricane-level wind speeds over the western Pacific Ocean with a satisfactory performance. In the future, we will collect data from additional hurricanes to test this retrieval model.

Acknowledgements This work was funded by the National Natural Science Foundation of China (Grant No. 61501433). The authors would like to thank the National Snow and Ice Data Center and the Japan Aerospace Exploration Agency for providing the AMSR2 brightness temperature data. The authors would like to thank the Hurricane Research Division for providing the SFMR data. SMAP data are produced by Remote Sensing Systems and sponsored by the NASA Earth Science funding. The authors declare that they have no conflict of interests regarding the publication of this paper.

References

Goodberlet M A, Swift C T, Wilkerson J C (1990). Ocean surface wind speed measurements of the Special Sensor Microwave/Imager (SSM/I). IEEE Trans Geosci Remote Sens, 28(5): 823–828

He J Y, Zhang S W, Wang Z Z (2015). Advanced microwave atmospheric sounder (AMAS) channel specifications and T/V calibration results on FY-3C Satellite. IEEE Trans Geosci Remote Sens, 53(1): 481–493

Krasnopolsky V M, Breaker L C, Gemmill W H (1995). A neural network as a nonlinear transfer function model for retrieving surface wind speeds from the special sensor microwave imager. J Geophys Res Oceans, 100(C6): 11033–11045

Meissner T, Ricciardulli L, Wentz F J (2016). Remote Sensing Systems SMAP daily Sea Surface Winds Speeds on 0.25 deg grid, Version 00.1 (BETA). Remote Sensing Systems, Santa Rosa, CA

Meissner T, Wentz F J (2009). Wind-vector retrievals under rain with passive satellite microwave radiometers. IEEE Trans Geosci Remote Sens, 47(9): 3065–3083

Quilfen Y, Prigent C, Chapron B, Mouche A A, Houti N (2007). The potential of QuikSCAT and WindSat observations for the estimation of sea surface wind vector under severe weather conditions. J Geophys Res Oceans, 112: C09023

Reul N, Tenerelli J, Chapron B, Chapron B, Vandemark D, Quilfen Y, Kerr Y (2012). SMOS satellite L-band radiometer: a new capability for ocean surface remote sensing in hurricanes. Journal of Geophysical Research: Oceans, 117: C02006

Roy C, Kovordányi R (2012). Tropical cyclone track forecasting techniques—A review. Atmos Res, 104–105: 40–69

Shibata A (2006). A wind speed retrieval algorithm by combining 6 and 10 GHz data from advanced microwave scanning radiometer: wind speed inside hurricanes. J Oceanogr, 62(3): 351–359

Uhlhorn E W, Black P G (2003). Verification of remotely sensed sea surface winds in hurricanes. J Atmos Ocean Technol, 20(1): 99–116

Uhlhorn E W, Black P G, Franklin J L, Goodberlet M, Carswell J, Goldstein A S (2007). Hurricane surface wind measurements from an operational stepped frequency microwave radiometer. Mon Weather Rev, 135(9): 3070–3085

Wentz F J (1997). A well-calibrated ocean algorithm for special sensor microwave/imager. J Geophys Res Oceans, 102(C4): 8703–8718

Wentz F J, Meissner T (2000). AMSR Ocean Algorithm, Algorithm Theoretical Basis Document. Remote Sensing Systems, 2000

Yan B H, Weng F Z (2008). Applications of AMSR-E measurements for tropical cyclone predictions part I: retrieval of sea surface temperature and wind speed. Adv Atmos Sci, 25(2): 227–245

Yueh S H (2008). Directional signals in WindSat observations of hurricane ocean winds. IEEE Trans Geosci Remote Sens, 46(1): 130–136

Yueh S H, Wilson W J, Dinardo S J, Hsiao S V (2006). Polarimetric microwave wind radiometer model function and retrieval testing for WindSat. IEEE Trans Geosci Remote Sens, 44(3): 584–596

Zabolotskikh E V, Mitnik L M, Chapron B (2014). GCOM-W1 AMSR2 and MetOp-A ASCAT wind speeds for the extratropical cyclones over the North Atlantic. Remote Sens Environ, 147: 89–98

Zabolotskikh E V, Mitnik L M, Reul N, Chapron B (2015). New possibilities for geophysical parameter retrievals opened by GCOM-W1 AMSR2. IEEE J Sel Top Appl Earth Obs Remote Sens, 8(9): 4248–4261

Zhang L, Wang Z Z, Shi H Q, Long Z Y, Du H D (2016a). Chaos particle swarm optimization combined with circular median filtering for geophysical parameters retrieval from WindSat. J Ocean Univ China, 15(4): 593–605

Zhang L, Yin X, Shi H, Wang Z Z (2016b). Hurricane wind speed estimation using WindSat 6 and 10 GHz brightness temperatures. Remote Sens, 8(9): 721